Journal of Medicinal Chemistry

pubs.acs.org/jmc

Article

Remdesivir Metabolite GS-441524 Effectively Inhibits SARS-CoV-2 Infection in Mouse Models

Yingjun Li,[#] Liu Cao,[#] Ge Li, Feng Cong, Yunfeng Li, Jing Sun, Yinzhu Luo, Guijiang Chen, Guanguan Li, Ping Wang, Fan Xing, Yanxi Ji, Jincun Zhao, Yu Zhang,* Deyin Guo,* and Xumu Zhang*

Cite This: https://dx.doi.org/10.1021/acs.jmedchem.0c01929

Read Online

ACCESS | Metrics & More | Article Recommendations | Supporting Information

ABSTRACT: The outbreak of coronavirus disease 2019 (COVID-19) has resulted in a global pandemic due to the rapid spread of severe acute respiratory syndrome coronavirus 2 (SARS-CoV-2). At the time of this manuscript's publication, remdesivir is the only COVID-19 treatment approved by the United States Food and Drug Administration. However, its effectiveness is still under question due to the results of the large Solidarity Trial conducted by the World Health Organization. Herein, we report that the parent nucleoside of remdesivir, GS-441524, potently inhibits the replication of SARS-CoV-2 in Vero E6 and other cell lines. Challenge studies in both an AAV-hACE2 mouse model of SARS-CoV-2 and in mice infected with murine hepatitis virus, a closely related coronavirus, showed that GS-441524 was highly efficacious in reducing the viral titers in CoV-infected organs without notable toxicity. Our results support that GS-441524 is a promising and inexpensive drug candidate for treating of COVID-19 and other CoV diseases.

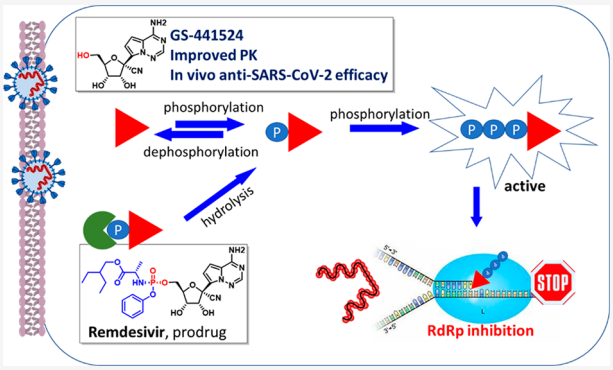

INTRODUCTION

Coronavirus disease 2019 (COVID-19) is caused by severe acute respiratory syndrome coronavirus 2 (SARS-CoV-2) and was first identified in December of 2019.[1,2] SARS-CoV-2 is a novel single-stranded RNA virus belonging to the Betacoronavirus genus.[3] Although most coronavirus infections cause only mild respiratory symptoms in humans, SARS-CoV-2 infections can progress to the acute respiratory distress syndrome (ARDS) and can be lethal.[4] Since the World Health Organization (WHO) declared COVID-19 as a global pandemic, COVID-19 infections and mortality have rapidly increased worldwide. As of October 24, 2020, there are more than 42 million confirmed COVID-19 cases and over 1 million associated deaths worldwide, according to Johns Hopkins University. Thus, effective therapies and drug candidates capable of treating COVID-19 are urgently needed.

Although several virus-based and host-based therapies have been evaluated for the treatment of COVID-19, such as lopinavir/ritonavir,[5] immunoglobulin, hydroxychloroquine,[6] EIDD-2801,[7] baricitinib,[8] and AT-527,[9] remdesivir is currently the only antiviral drug that has received the U.S. Food and Drug Administration (FDA) approval for treating COVID-19.[10−14] Remdesivir was granted FDA approval for COVID-19 due to encouraging results from a randomized, double-blind placebo-controlled trial conducted by the National Institutes of Health (NIH).[15,16] However, results demonstrating no significant reduction in mortality with remdesivir treatment in a larger clinical trial conducted by the WHO have caused many to question the efficacy of remdesivir.[17] This shortcoming has been exacerbated by its expensiveness and its difficult synthesis, which especially limits its broad applicability and accessibility in developing countries. Structurally, remdesivir is a nucleotide McGuigan prodrug that was designed for the intracellular delivery of a nucleoside monophosphate analogue;[18,19] this is then phosphorylated to give the active nucleoside triphosphate analogue (GS-443902).[20] As a McGuigan prodrug, the anionic phosphate moiety on remdesivir is masked by phenol and an L-alaninate ethylbutyl ester, which is intended for intracellular enzymatic removal.[21,22] However, pharmacokinetics (PK) studies in nonhuman primates (NHP) and healthy human subjects following intravenous (IV) administration of remdesivir show that remdesivir is rapidly metabolized to GS-704277 before releasing the parent nucleoside, GS-441524, which persists in circulation (Figure 1).[23−27] As the major metabolite of remdesivir, GS-441524 demonstrated persistent plasma exposure and a significantly longer half-life and area under the

Special Issue: COVID-19

Received: November 7, 2020

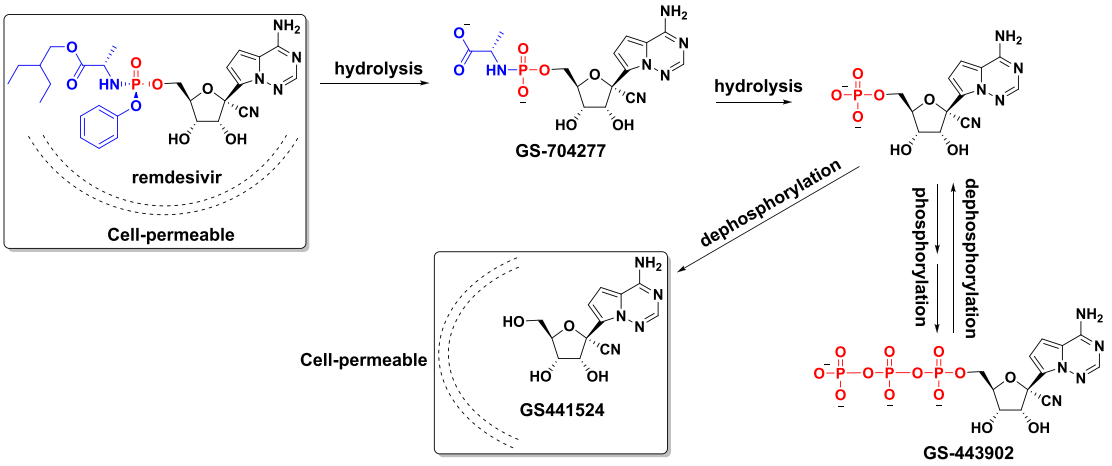

Figure 1. Remdesivir metabolism with chemical structures of metabolites.

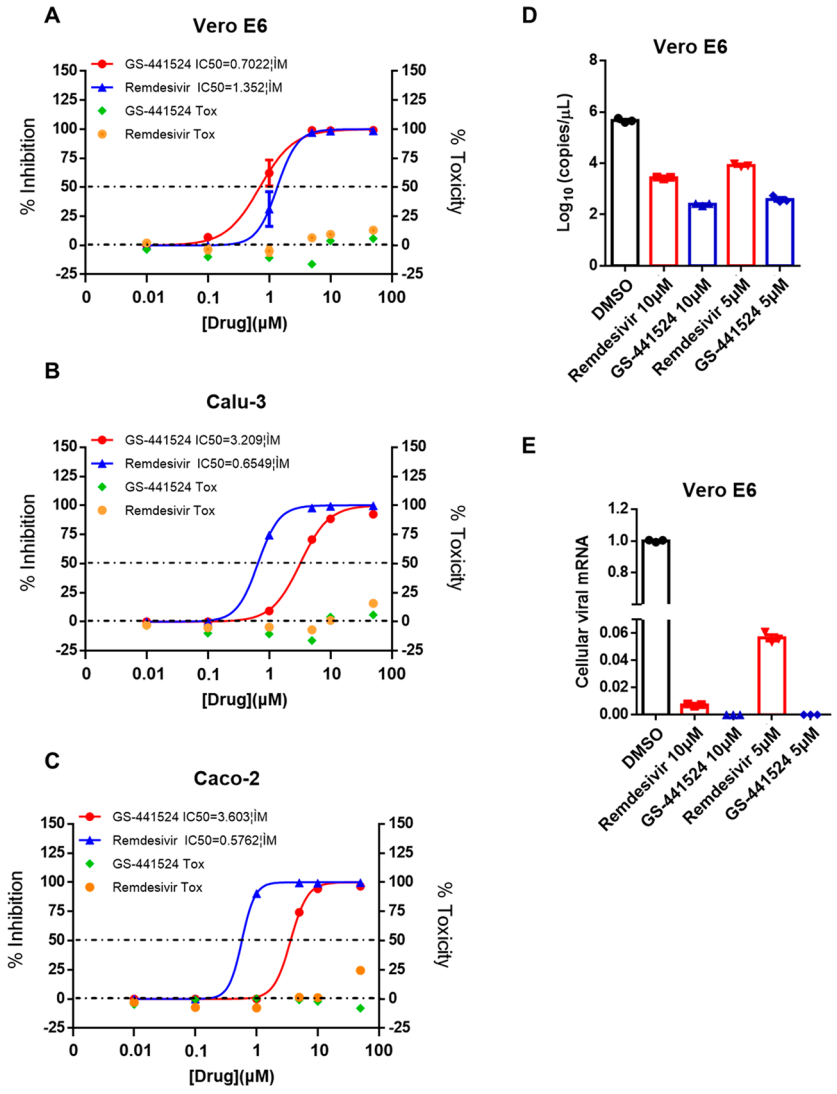

Figure 2. Remdesivir and GS-441524 potently inhibit SARS-CoV-2 replication in vitro. Vero E6 (A), Calu-3 (B), and Caco-2 (C) were infected with SARS-CoV-2 at an MOI of 0.05 and treated with dilutions of either GS-441524 or remdesivir (0, 0.01, 0.1, 1, 5, 10, 50 μM) for 48 h. Viral yield in the cell supernatant was then quantified by qRT-PCR. Data represented are the mean value of % inhibition of SARS-CoV-2 in cells. Cytotoxicity of GS-441524 (green dots) and remdesivir (orange dots) was determined using a CCK-8 test. Vero E6 cells were infected with SARS-CoV-2 at an MOI of 0.05 and treated with dilutions of the indicated compounds for 48 h. Viral RNA in the cell supernatant (D) and pellet (E) was then quantified by qRT-PCR.

https://dx.doi.org/10.1021/acs.jmedchem.0c01929
J. Med. Chem. XXXX, XXX, XXX−XXX

curve (AUC) value ($t_{1/2} \approx 27$ h, AUC = 2230 h·ng/mL) compared to remdesivir ($t_{1/2} < 1$ h, AUC = 1590 h·ng/mL).[24,25] The extent to which the remdesivir metabolites, especially GS-441524, contribute to the cumulative anti-SARS-CoV-2 activity of remdesivir remains unclear.

In vitro studies have shown that GS-441524 is significantly less potent against HeLa and Huh-7 cells infected with either Ebola virus (EBOV) or respiratory syncytial virus (RSV) compared to remdesivir.[12,28] Activation of GS-441524 requires two phosphorylation steps for conversion to its pharmacologically active triphosphate (GS-443902). Initial conversion of nucleosides such as GS-441524 to the monophosphate is considered to be rate-limiting;[29] remdesivir was designed to bypass the initial phosphorylation step.[30] Nevertheless, GS-441524 exhibited good in vitro efficacy against human CoVs such as SARS-CoV, middle east respiratory syndrome coronavirus (MERS-CoV), and other zoonotic coronaviruses.[31] Extensive in vitro and in vivo testing of GS-441524 has been conducted in the context of feline infectious peritonitis (FIP), which is caused by feline coronavirus (FCoV), a closely related coronavirus. Though FIP has long been considered a uniformly fatal disease in cats, FIP-afflicted cats administered GS-441524 were successfully treated with an up to 96% cure rate.[32,33] These studies indicate the potential of GS-441524 for treating coronavirus diseases such as COVID-19.[34,35] Here, we investigate the hypothesis that GS-441524 could be effective for treating COVID-19. We compare the anti-SARS-CoV-2 activities of GS-441524 and remdesivir in vitro, examine the PK profile in rodents, and evaluate the in vivo efficacy of GS-441524 in mice infected with either SARS-CoV-2 or murine hepatitis virus (MHV). Our results provide further experimental evidence that GS-441524 is a promising antiviral compound for COVID-19 and other emerging CoV diseases.

RESULTS AND DISCUSSION

GS-441524 and Remdesivir Potently Inhibit SARS-CoV-2 Replication. Initially, we compared the anti-SARS-CoV-2 activities of GS-441524 and remdesivir in the following cell lines: Vero E6 (African green monkey kidney), Calu-3 (human lung adenocarcinoma), and Caco-2 (colorectal adenocarcinoma). Cells were infected with SARS-CoV-2 at a multiplicity of infection (MOI) of 0.05 and treated with dilutions of either remdesivir or GS-441524. Antiviral activities were evaluated by quantitative real-time polymerase chain reaction (qRT-PCR) quantification of a viral copy number in the supernatant 48 h post infection. GS-441524 and remdesivir potently inhibited SARS-CoV-2 replication in a dose-dependent manner (Figure 2). Consistent with previous reports,[34] GS-441524 demonstrated slightly greater anti-SRAR-COV-2 activity (half-maximal inhibitory concentration (IC_{50}) = 0.70 μM) compared to remdesivir (IC_{50} = 1.35 μM) in Vero E6 cells. Comparison of the intracellular viral RNA load in Vero E6 cells showed a similar trend in antiviral activities of GS-441524 and remdesivir to that observed in the supernatant (Figure 2d,e). In Calu-3 and Caco-2 cells, remdesivir demonstrated greater potency compared to GS-441524, with IC_{50} values of 0.65 and 0.58 μM versus 3.21 and 3.62 μM for each cell line, respectively. Our results are consistent with previous reports, which suggest that the relative potencies of GS-441524 and remdesivir are cell-type dependent.[34] Both GS-441524 and remdesivir were also evaluated for their cytotoxic potential using the CCK-8 assay. At concentrations up to 50 μM, treatment with GS-441524 did not reduce cell viability, indicating a good safety profile (Figure 2a–c).

Pharmacokinetic Profile of GS-441524 in Rat. While the PK profiles of remdesivir and its metabolites have been extensively studied following IV administration in NHP and human,[25,36] PK studies after direct administration of GS-441524 have not been conducted when this manuscript was prepared. Thus, we performed PK studies of GS-441524 in Sprague-Dawley (SD) rats via IV and intragastric (IG) administration of GS-441524 at 30 mg/kg over 48 h (Figure 3). Following IV administration, GS-441524 exhibited

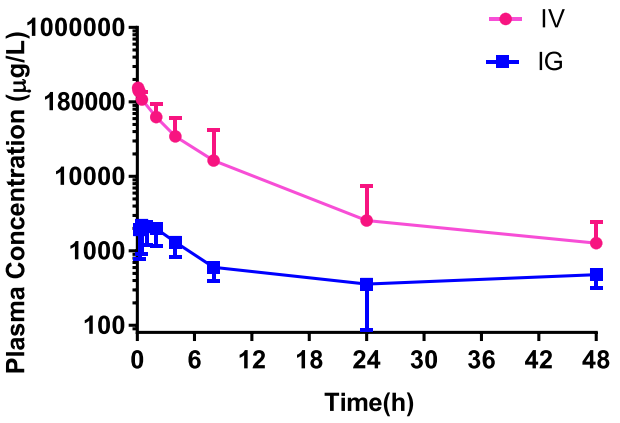

Figure 3. The time–concentration curve of GS-441524 in a PK study. Plasma concentration and time curve following IV (red) and IG (blue) administration of 30 mg/kg GS-441524 in SD rat (data indicated are mean ± SD, N = 4).

favorable PK parameters, with a long $t_{1/2}$ of 4.8 h and a high C_{max} of 163 616.6 μg/L. Following IG administration, we found that GS-441524 had a bioavailability of ~5%. The PK values over 48 and 24 h (Table S2) are different from a recent disclosed PK value of GS-441524, probability due to the differences in dosage and drug formulation (Table 1).[37]

Table 1. Pharmacokinetics Parameters of GS-441524 over 48 h in Rat[a]

	GS-441524 (IV)	GS-441524 (IG)
AUC(0-t) (μg/L·h)	591 916 ± 265 802	28 668 ± 7062
$t_{1/2}$[b] (h)	4.77 ± 2.33	20.55 ± 16.43
T_{max} (h)	0.10 ± 0.04	0.94 ± 0.77
C_{max} (μg/L)	163 616.6 ± 3747.3	2708.0 ± 1308.8
F%		4.84 ± 1.19

[a]Each group had four rats. [b]$t_{1/2}$ was calculated as the terminal elimination half-life.

GS-441524 Inhibits SARS-CoV-2 in AAV-hACE2 Transduced Mice. Next, we studied the anti-SARS-CoV-2 of GS-441524 in vivo. Although mice are convenient models for in vivo drug testing, they are resistant to SARS-CoV-2. SARS-CoV-2 uses human angiotensin-converting enzyme 2 (ACE2) to enter cells, but mouse ACE2 does not sensitize cells to infection.[3] We generated transduction mice with adenovirus associated virus (AAV) vector expressing hACE2 laboratory, supporting SARS-CoV-2 infection and pathogenesis.[38] Mice were inoculated intranasally with 1×10^5 plaque forming units (PFU) of SARS-CoV-2 in Biosafety Level 3 (BSL-3), and body

https://dx.doi.org/10.1021/acs.jmedchem.0c01929
J. Med. Chem. XXXX, XXX, XXX–XXX

weights were monitored over 10 d as an indicator of overall health.[38,39] GS-441524 was administered intraperitonially (IP) at 25 mg/kg 1 d prior to infection and was continued for 8 d (Figure 4a). Compared to SARS-CoV-2-infected mice treated

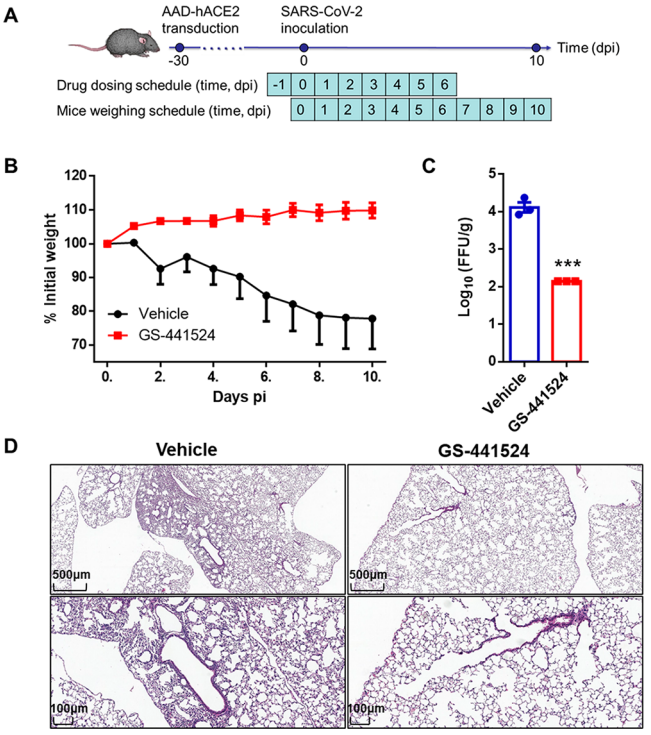

Figure 4. Anti-SARS-CoV-2 efficacy of GS-441524 in an AAV-hACE2 mouse model. AAV-hACE2 transduced mice were infected with SARS-CoV-2. Mice were administrated either vehicle or GS-441524 (25 mg/kg/day) at −1 dpi and were treated for a total of 8 d. (A) Changes in body weight for either vehicle (black) or GS-441524-treated (red) mice. (B) Viral titers from lung tissue of three mice per group were harvested at 2 dpi and analyzed by FFA. ***p-value ≤ 0.0005. (C) Representative H&E staining of lungs from hACE2 transduced mice. (D) Scale bars, 500 μm (top) and 100 μm (bottom).

with GS-441524, vehicle-treated mice were characterized by significant weight loss (more than 20%), severe pulmonary pathology, and high-titer viral replication in the lungs (Figure 4). Mice treated with GS-441524 demonstrated significant virus clearance in the lungs at 2 d post inoculation (dpi) and did not experience weight loss. Vehicle-treated mice demonstrated multiple injuries, including inflammatory cell infiltration ranging from the trachea, peri-alveolar space, to the interstitium. Together, these data provide the first solid demonstration of the efficacy of GS-441524 against SARS-CoV-2 in vivo.

Efficacy of GS-441524 in Mice Infected with MHV. MHV belongs to the coronavirus family of RNA viruses, sharing a common genus with SARS-CoV-2.[40] MHV-A59 (A59 strain of MHV) infection causes hepatitis in mice. Because MHV is a both a naturally occurring pathology in mice and closely related to SARS-CoV-2, MHV-infected mice could serve as a rapid experimental model to evaluate anti-CoV agents. The active triphosphate of remdesivir and GS-441524, GS-443902, has already been demonstrated to be an effective inhibitor of the MHV RdRp in vitro.[33,38] However, there are currently no reports on the in vivo efficacy of GS-441524 in MHV-infected mice.

To gain insight into the in vivo safety and efficacy of GS-441524 against MHV, mice were intranasally inoculated with MHV-A59 and were randomly assigned to one of six groups: Group A: infected, untreated control; Group B1:100 mg/kg GS-441524 IG 0.5 h post infection (hpi), then 50 mg/kg daily in infected mice; Group B2:100 mg/kg GS-441524 IP 0.5 hpi, then 50 mg/kg daily in infected mice; Group C1: B2 matched control in uninfected mice; Group C2: B2 matched control in uninfected mice; Group D: uninfected control. In Group A, ∼87.5% of mice died at 7 dpi (Figure 5a, group A). MHV-infected mice treated with GS-441524 in Groups B1 and B2 demonstrated significant improvement in survival, which highlights the potent, anti-MHV activity of GS-441524 (Figure 5a, groups B1 and B2). In contrast to the 12.5% survival of infected controls in Group A, mice treated either IG or IP in Groups B1 and B2 demonstrated 100% survival.

MHV largely manifests as a liver pathology.[41] To examine the relationship between the potent, observed antiviral activity of GS-441524 in MHV and the tissue distribution of GS-441524 in mice, viral titers in the liver were analyzed. RNA was extracted from liver tissue for qRT-PCR analysis at 3 dpi of MHV-infected mice (Groups A, B1, and B2). Treatment with GS-441524, either IG or IP, resulted in a greater than 99.9% viral inhibition compared to untreated controls (Figure 5c,d). Moreover, the dose of GS-441524 administered was demonstrated to be safe, as indicated by the minimal changes in body weight (Groups C1 and C2) compared to blank controls (Group D; Figure 5b). Though treatment with GS-441524 significantly reduced viral titers and improved the survival of MHV-infected mice, mice in Groups B1 and B2 still experienced a similar degree of weight loss as untreated mice in Group A (Figure 5b). The weight loss of these virus-inoculated groups may be due to the consequences of infection. Both the safety profile of GS-441524 in uninfected mice and the pattern of weight loss observed in MHV-infected mice were readily reproduced in a repeated study (Figure S2).

CONCLUSIONS

COVID-19 is associated with high contagiousness, morbidity, and mortality, emphasizing the imperative need for antiviral agents. While remdesivir demonstrated accelerated recovery in adults hospitalized with COVID-19 in a large randomized clinical trial and is FDA-approved for the treatment of COVID-19, its efficacy is still under question.[15,17,42] Because of its synthetic complexity, costliness, and obligatory IV administration, application of and accessibility to remdesivir will be limited. These shortcomings, coupled with a careful pharmacokinetic evaluation,[35] suggest that the parent nucleoside GS-441524 is superior to remdesivir for COVID-19 treatment in several aspects. First, GS-441524 is structurally simpler and easier to synthesize compared to remdesivir (Scheme S1). Second, preclinical and clinical PK studies of remdesivir have revealed that GS-441524 is already the predominant and persistent metabolite in circulation. Although other metabolites, such as the alanine metabolite GS-704277, were also detected in plasma, GS-704277 is negatively charged, poorly cell permeable, and rapidly excreted from the body (Figure 1).[43] Third, GS-441524 demonstrated potent antiviral activity against several strains of coronaviruses. However, even with these advantages, primary human airway epithelial (HAE) cells infected with SARS-CoV-2 were reported to be much

https://dx.doi.org/10.1021/acs.jmedchem.0c01929
J. Med. Chem. XXXX, XXX, XXX−XXX

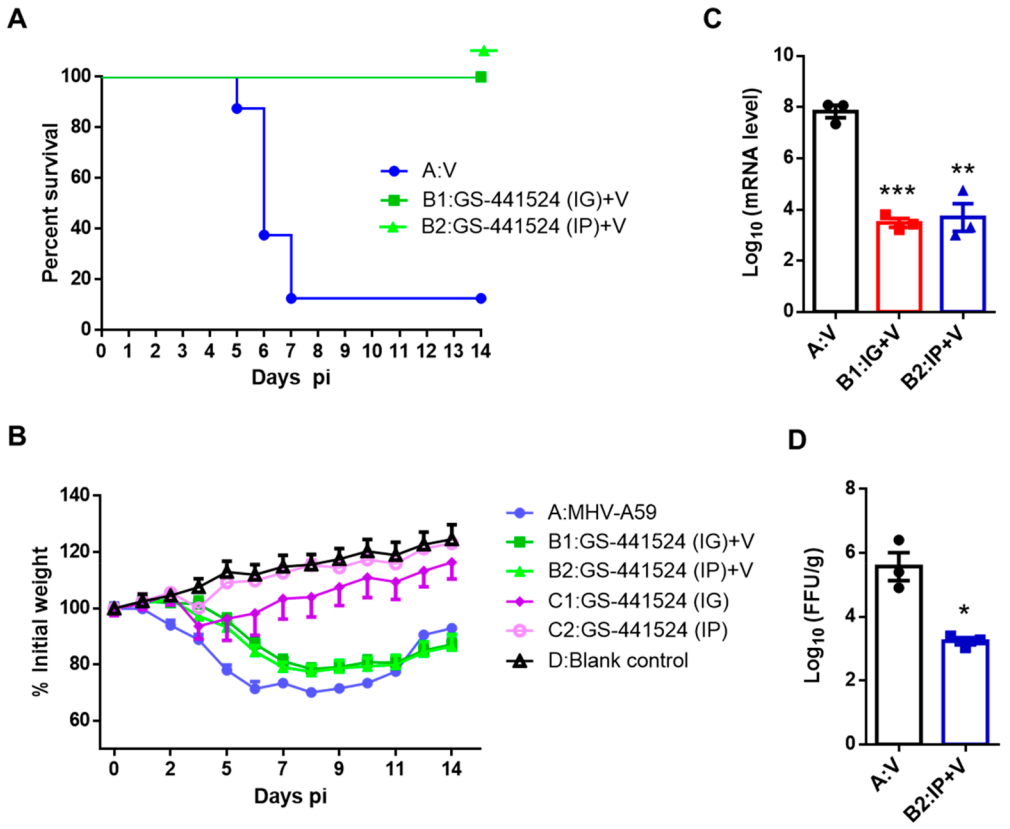

Figure 5. Antiviral efficacy of GS-441524 in mice with MHV-A59: Mice were randomly divided into six groups: Group A: MHV-A59 infected, untreated control; Group B1:100 mg/kg GS-441524 IG 0.5 hpi, then 50 mg/kg daily in infected mice; Group B2:100 mg/kg GS-441524 IP 0.5 hpi, then 50 mg/kg daily in infected mice; Group C1: B2 matched control in uninfected mice; Group C2: B2 matched control in uninfected mice; Group D: uninfected control. Note: V = virus. (A) Survival curves of mice in Groups A (blue), B1 (dark green), and B2 (light green). Note: $N = 8$ per group. (B) Body weights of animals in the six groups; Note: $N = 8$ per group. (C) Viral titers in the liver of mice from Group A (black), Group B1 (red), and Group B2 (blue) quantified by qRT-PCR ($N = 3$ per group) at 3 dpi. (D) Viral titers in the liver of mice from Group A (black) and Group B2 (blue) were quantified by focus forming assay (FFU; $N = 3$ per group) at 3 dpi. *p-value $\leq$ 0.05; **p-value $\leq$ 0.005; ***p-value $\leq$ 0.0005.

more sensitive to remdesivir than GS-441524, questioning the potential efficacy of GS-441524 in COVID-19-infected lung tissue.[34]

Herein, we report the in vitro and in vivo anti-SARS-CoV-2 activities of GS-441524. GS-441524 effectively inhibited SARS-CoV-2 in three cell lines (Vero E6, Calu-3, and Caco-2). In a lethal MHV-A59 mouse model, GS-441524 administered either IP or IG was capable of reducing viral loads in the liver and preventing death (Figure 5). Treatment with GS-441524 in AAV-hACE2 mice infected with SARS-CoV-2 resulted in significant reductions in viral titers compared to untreated controls (Figure 4b). We showed that GS-441524 potently inhibits SARS-CoV-2 replication in the lungs and alleviates lung inflammation and injury (Figure 4c). These data strongly suggest that GS-441524 could have an antiviral efficacy in human lung tissue infected with COVID-19 and highlight the differences between in vitro HAE cultures and intact respiratory epithelial cells in vivo. Moreover, GS-441524 showed minimal cytotoxicity and in vivo toxicity, supporting previous reports of its remarkable safety profile.[12,20] The potent in vivo efficacy of GS-441524 against SARS-CoV-2 and MHV in mouse models reported here, together with its robust clinical activity against feline coronavirus,[32,33,44] demonstrate its broad utility against zoonotic and human CoVs and the ability for GS-441524 to be bioconverted to the active triphosphate, GS-443902, across different tissues. In sum, our results strongly suggest that part of remdesivir's therapeutic effects arise from the metabolite GS441524 and that the added structural complexity of the phosphate prodrug on remdesivir may be unnecessary. Taken together, our results support GS-441524 as a safe and cheaper antiviral compared to remdesivir and is a promising drug candidate for the treatment of COVID-19 and emerging coronavirus diseases in the future.

EXPERIMENTAL SECTION

Compounds, Cells, and Viruses. Remdesivir (Catalog (Cat.) No. T7766) was purchased from TargetMol, and GS-441524 (Cat. No. BCP35590) was purchased from Biochempartner. GS-441524 was diluted in 10% dimethyl sulfoxide (DMSO), 10% Tween 80, and 80% saline for in vivo studies. African green monkey kidney Vero E6 cell line (Vero E6) was kindly provided by Dr. Hui Zhang (Sun Yat-sen University). Calu-3 and Caco-2 were kindly provided by Dr. Yu Chen (Wuhan University). Vero E6 and Caco-2 were cultured in Dulbecco's Modified Eagle's Medium (DMEM) supplemented with 10% fetal bovine serum (FBS), and 100 U/mL penicillin and streptomycin at 37 °C in a humidified atmosphere of 5% CO_2. Calu-3 cells were cultured in DMEM supplemented with 20% FBS, 100 U/mL penicillin and streptomycin, and 1% nonessential amino acid (NEAA) cell culture at 37 °C in a humidified atmosphere of 5% CO_2. SARS-CoV-2 (hCoV-19/CHN/SYSU-IHV/2020 strain, Accession ID on GISAID: EPI_ISL_444969) was isolated from a sputum sample from a woman admitted to the Eighth People's Hospital of Guangzhou. MHV-A59 was obtained from the American Type Culture Collection. MHV-A59 was expanded in mouse liver cells

https://dx.doi.org/10.1021/acs.jmedchem.0c01929
J. Med. Chem. XXXX, XXX, XXX−XXX

NCTC 1469. Supernatants were collected, and a passage 7 stock was subsequently stored at −80 °C until used. SARS-CoV-2 infection experiments were performed in the BSL-3 laboratory of Sun Yat-sen University or Guangzhou Customs District Technology Center. MHV-A59 infection experiments were performed in the Biosafety Level 2 (BSL-2) laboratory of Guangdong Laboratory Animals Monitoring Institute. All animal studies protocols were approved by the Animal Welfare Committee, and all procedures used in animal studies complied with the guidelines and policies of the Animal Care and Use Committee.

Antiviral Activity Assays. Vero E6, Calu-3, and Caco-2 cells were seeded at 1×10^5 cells per well in 24-well plates. Cells were allowed to adhere for 16−24 h and then infected at an MOI of 0.05 with SARS-CoV-2 for 1 h at 37 °C. Then the viral inoculum was removed, and the cells were washed two times with prewarmed phosphate-buffered saline (PBS). A medium containing dilutions of remdesivir, GS-441524, or DMSO was added. At 48 hpi, supernatants or cells were harvested for qRT-PCR analysis. The dose−response curves were plotted from viral RNA copies versus the drug concentrations using GraphPad Prism 6 software.

qRT-PCR Analysis. For SARS-CoV-2 supernatant RNA quantification, the RNA was isolated by an E.Z.N.A.Viral RNA Kit (OMEGA). A SARS-CoV-2 nucleic acid detection kit (Daan Company) was used to detect the virus. For the detection of cellular viruses and tissue viruses, the total RNA was isolated from cells or tissue samples with TRIzol reagent under the instruction of the manufacturer. The mRNAs were reverse transcribed into cDNA by PrimeScript RT reagent Kit (Takara). The cDNA was amplified by a fast two-step amplification program using ChamQ Universal SYBR qPCR Master Mix (Vazyme Biotech Co., Ltd.). Glyceraldehyde 3-phosphate dehydrogenase (GAPDH) was used to normalize the input samples via the ΔΔCT method. The relative mRNA expression level of each gene was normalized to GAPDH housekeeping gene expression in the untreated condition, and fold induction was calculated by the ΔΔCT method relative to those in untreated samples.

CCK-8 Cell Viability Assay. To investigate the effect of drugs on cell viability, Vero E6, Calu-3, and Caco-2 cells were seeded in 96-well plates at a density of 20 000 cells/well and were treated with drugs at indicated concentrations (0, 0.01, 0.1, 1, 5, 10, 50 μM) for 48 h. The cell viability was tested by using a Cell Counting Kit-8 (CCK-8, Bimake, B34302). The figures were plotted from viral RNA copies in supernatants versus the drug concentrations using GraphPad Prism 6 software.

PK Analysis. SD rats (male, four animals per group) weighing 180−220 g were injected with GS-441514 intravenously and intragastrically at a dose of 30 mg/kg. After administration, 0.3 mL of the orbital blood was taken at 0.083, 0.16, 0.25, 0.5, 2, 3, 4, 8, 24, and 48 h for the IV group and at 0.25, 0.5, 1, 2, 3.0, 4, 6, 8, 24, and 48 h for the IG group. Samples were centrifuged under 4000 rpm/min for10 min at 4 °C. The supernatants (plasma) were collected and stored at −20 °C for future analysis. For plasma drug concentration analysis, an aliquot of 50 ul of each plasma sample was treated with 100ul of 90% methanol and 600 ul of a 50% acetonitrile mixture. The samples were centrifuged under 1200 rpm for 10 min and filtered through 0.2 μm membrane filters. The drug concentration in each sample was tested by high-performance liquid chromatography (HPLC)/mass spectrometry (MS). Analytes were separated on an InertSustain AQ-C18HP column (3.0 mm× 50 mm, 3.0 μm, GL) using Waters UPLC/XEVO TQ-S. The pharmacokinetic parameters were calculated using DAS (Drug and Statistics) 3.0 software. The time−concentration curve was plotted using GraphPad Prism 6 software.

AAV-HACE2 SARS-CoV-2 Infected Mice Study. Adeno-associated virus 9 encoding hACE2 was purchased from Packgene (AAV-hACE2). The modified intratracheal aerosolization was used to intratracheally deliver AAV vector (5×10^{11} GC) to lung tissue of four-week-old BALB/c mice.[39,45] Briefly, the mice were anesthetized with 2.5% isoflurane in O_2 (1 L/min). The 50 μL AAV solution was then aerosolized at a rate of ∼15 μL/second using a microsprayer under fiberoptic laryngoscope. The mice were further maintained with anesthesia for 5 min to promote the delivery of the vector deep into the lungs before transferring back to the cage. Thirty days post transduction, the mice were intranasally infected with SARS-CoV-2 (1×10^5 PFU) in a total volume of 50 μL of DMEM. Immediately, they were randomly divided into two groups (each group had nine mice). A dosage of 25 mg/kg/d of GS-441524 or vehicle was IP administrated to the mice beginning at −1 dpi for a consecutive 8 d period. Mice were monitored and weighed daily for 8 d consecutively beginning at 0 dpi. Four mice of each group were dissected at 2 dpi to collect lung tissues for virus titer detection and HE staining.

Focus Forming Assay (FFA). The viral titration in lung or liver tissue was determined using FFA assay as previously described.[39] Vero E6 cells were seeded in 96-well plates 1 d before infection. Tissue homogenates were serially diluted and used to inoculate Vero E6 cells at 37 °C for 1 h. Inocula were then removed before the addition of 125 μL of 1.6% carboxymethylcellulose per well and warmed to 37 °C. After 24 h, cells were fixed with 4% paraformaldehyde and permeabilized with 0.2% Triton X-100. The cells were then incubated with a rabbit anti-SARS-CoV-2 nucleocapsid protein polyclonal antibody (Cat. No. 40143-T62, Sino Biological), followed by an HRP-labeled goat antirabbit secondary antibody (Cat. No. 109-035-088, Jackson ImmunoResearch Laboratories). The foci were visualized by TrueBlue Peroxidase Substrate (KPL) and counted with an ELISPOT reader (Cellular Technology). Viral titers were calculated as per gram tissue.

H&E Staining. Mice lung dissections were fixed in zinc formalin and embedded with paraffin. Tissue sections (∼4 μm) were stained with hematoxylin and eosin.

Mouse MHV Efficacy Study. Three to four weeks old specific-pathogen-free (SPF) male BALB/c mice (Guangdong Medical Experimental Animal Center) were maintained in microisolated cages and housed in the animal colony at the biosafety level 2 facility at Guangdong Laboratory Animals Monitoring Institute. Mice were fed standard lab chow diet and water ad libitum. The mice were randomly divided into eight groups and anesthetized by respiration with isoflurane. Immediately, mice in Group A, B1, and B2 received an intranasal inoculation of 30 μL of MHV-A59 (median tissue culture infectious dose ($TCID_{50}$) = $10^{-7.125}$/100 μL) in PBS. Control groups (Groups C1, C2, and D, each group having three mice) were mock-treated with phosphate-buffered saline. Mice in the B1 and B2 groups received GS-441524 via IG (Group B1) or IP (Group B2) at 0.5 hpi at a dose of 100 mg/kg, and mice in A group received PBS instead. Mice in the control groups (Groups C1, C2, and D) received GS-441524 or PBS in the same way. GS-441524 was administered at 50 mg/kg once a day in the following 4 d. Groups A and D administered 0.2 mL of PBS. Mice were monitored daily for symptoms of disease, including body weights, clinical symptoms, and death, for14 d. Three mice of groups A, B1, and B2 were dissected at 3 dpi to collect liver tissues for virus titration detection.

Statistical Analysis. All values are mean ± standard deviation (SD) or standard error of measure (SEM) of individual samples. Data analysis was performed with GraphPad Prism Software (GraphPad Software Inc., version 6.01). The statistical tests utilized are two-tailed, and the respective details have been indicated in figure legends. *p*-Values of less than 0.05 were considered statistically significant. (*, *p*-value of ≤0.05. **, *p*-value of ≤0.005. ***, *p*-value of ≤0.0005. ****, *p*-value of ≤0.0001).

■ ASSOCIATED CONTENT

Supporting Information

The Supporting Information is available free of charge at https://pubs.acs.org/doi/10.1021/acs.jmedchem.0c01929.

The comparison of synthesis of remdesivir and GS-441524, primers sequence, PK data of GS-441524 over 24 h in rat, and additional MHV animal study (PDF)

https://dx.doi.org/10.1021/acs.jmedchem.0c01929
J. Med. Chem. XXXX, XXX, XXX−XXX

AUTHOR INFORMATION

Corresponding Authors

Yu Zhang − *Guangdong Province Key Laboratory of Laboratory Animals, Guangdong Laboratory Animals Monitoring Institute, Guangzhou, Guangdong 510663, China*; Email: zhy@gdlami.com

Deyin Guo − *Centre for Infection and Immunity Studies, School of Medicine, Sun Yat-sen University, Shenzhen, Guangdong 518107, China*; Email: guodeyin@mail.sysu.edu.cn

Xumu Zhang − *Shenzhen Key Laboratory of Small Molecule Drug Discovery and Synthesis, Department of Chemistry, College of Science and Medi-X, Academy for Advanced Interdisciplinary Studies, Southern University of Science and Technology, Shenzhen, Guangdong 518055, China*; orcid.org/0000-0001-5700-0608; Email: zhangxm@sustech.edu.cn

Authors

Yingjun Li − *Shenzhen Key Laboratory of Small Molecule Drug Discovery and Synthesis, Department of Chemistry, College of Science and Medi-X, Academy for Advanced Interdisciplinary Studies, Southern University of Science and Technology, Shenzhen, Guangdong 518055, China*

Liu Cao − *Centre for Infection and Immunity Studies, School of Medicine, Sun Yat-sen University, Shenzhen, Guangdong 518107, China*

Ge Li − *Guangdong Province Key Laboratory of Laboratory Animals, Guangdong Laboratory Animals Monitoring Institute, Guangzhou, Guangdong 510663, China*

Feng Cong − *Guangdong Province Key Laboratory of Laboratory Animals, Guangdong Laboratory Animals Monitoring Institute, Guangzhou, Guangdong 510663, China*

Yunfeng Li − *Guangdong Province Key Laboratory of Laboratory Animals, Guangdong Laboratory Animals Monitoring Institute, Guangzhou, Guangdong 510663, China*

Jing Sun − *State Key Laboratory of Respiratory Disease, National Clinical Research Center for Respiratory Disease, Guangzhou Institute of Respiratory Health, The First Affiliated Hospital of Guangzhou Medical University, Guangzhou, Guangdong 510182, China*

Yinzhu Luo − *Guangdong Province Key Laboratory of Laboratory Animals, Guangdong Laboratory Animals Monitoring Institute, Guangzhou, Guangdong 510663, China*

Guijiang Chen − *Guangdong Province Key Laboratory of Laboratory Animals, Guangdong Laboratory Animals Monitoring Institute, Guangzhou, Guangdong 510663, China*

Guanguan Li − *Shenzhen Key Laboratory of Small Molecule Drug Discovery and Synthesis, Department of Chemistry, College of Science, Southern University of Science and Technology, Shenzhen, Guangdong 518055, China*; orcid.org/0000-0002-2284-0348

Ping Wang − *Shenzhen Key Laboratory of Small Molecule Drug Discovery and Synthesis, Department of Chemistry, College of Science, Southern University of Science and Technology, Shenzhen, Guangdong 518055, China*

Fan Xing − *Centre for Infection and Immunity Studies, School of Medicine, Sun Yat-sen University, Shenzhen, Guangdong 518107, China*

Yanxi Ji − *Centre for Infection and Immunity Studies, School of Medicine, Sun Yat-sen University, Shenzhen, Guangdong 518107, China*

Jincun Zhao − *State Key Laboratory of Respiratory Disease, National Clinical Research Center for Respiratory Disease, Guangzhou Institute of Respiratory Health, The First Affiliated Hospital of Guangzhou Medical University, Guangzhou, Guangdong 510182, China*

Complete contact information is available at: https://pubs.acs.org/10.1021/acs.jmedchem.0c01929

Author Contributions

#(Y.-J.L. and L.C.) These authors contributed equally to this work.

Notes

The authors declare no competing financial interest.

ACKNOWLEDGMENTS

The project was supported by Shenzhen Science and Technology Innovation Committee (ZDSYS20190-902093215877), Shenzhen Science and Technology Program (JSGG20200225150431472 & KQTD20180411143323605), Shenzhen Bay Laboratory (SZBL2019062801006), and Technology and National Natural Science Foundation of China (Grant Nos. 32041002 & 81620108020). D.G. is also supported by Guangdong Zhujiang Talents Program and National Ten-thousand Talents Program. We thank Dr. C.-W. Lin from School of Medicine, Sun Yat-Sen University, for the help in lung pathology analysis.

ABBREVIATIONS USED

COVID-19, Coronavirus disease 2019; SARS-CoV-2, severe acute respiratory syndrome coronavirus 2; FDA, U.S. Food and Drug Administration; MHV, murine hepatitis virus; AAV, adenovirus associated virus; hACE2, Angiotensin-converting enzyme 2; WHO, World Health Organization; RdRP, RNA-dependent RNA polymerase; CoV, Coronavirus; NHP, nonhuman primates; EBOV, ebola virus; HCV, hepatitis C virus; RSV, respiratory syncytial virus; FIP, Feline infectious peritonitis; FCoV, feline coronaviruses; PK, Pharmacokenetics; IC_{50}, half maximal inhibitory concentration; SD, standard deviation; PFU, plaque forming unit; pi, post inoculation; FFU, Focus-forming unit; H&E, hematoxylin-eosin

REFERENCES

(1) Huang, C.; Wang, Y.; Li, X.; Ren, L.; Zhao, J.; Hu, Y.; Zhang, L.; Fan, G.; Xu, J.; Gu, X.; Cheng, Z.; Yu, T.; Xia, J.; Wei, Y.; Wu, W.; Xie, X.; Yin, W.; Li, H.; Liu, M.; Xiao, Y.; Gao, H.; Guo, L.; Xie, J.; Wang, G.; Jiang, R.; Gao, Z.; Jin, Q.; Wang, J.; Cao, B. Clinical features of patients infected with 2019 novel coronavirus in Wuhan, China. *Lancet* **2020**, *395*, 497−506.

(2) Mason, R. J. Pathogenesis of COVID-19 from a cell biology perspective. *Eur. Respir. J.* **2020**, *55*, 2000607.

(3) Zhou, P.; Yang, X.-L.; Wang, X.-G.; Hu, B.; Zhang, L.; Zhang, W.; Si, H.-R.; Zhu, Y.; Li, B.; Huang, C.-L.; Chen, H.-D.; Chen, J.; Luo, Y.; Guo, H.; Jiang, R.-D.; Liu, M.-Q.; Chen, Y.; Shen, X.-R.; Wang, X.; Zheng, X.-S.; Zhao, K.; Chen, Q.-J.; Deng, F.; Liu, L.-L.; Yan, B.; Zhan, F.-X.; Wang, Y.-Y.; Xiao, G.-F.; Shi, Z.-L. A pneumonia outbreak associated with a new coronavirus of probable bat origin. *Nature* **2020**, *579*, 270−273.

(4) Li, Q.; Guan, X.; Wu, P.; Wang, X.; Zhou, L.; Tong, Y.; Ren, R.; Leung, K. S. M.; Lau, E. H. Y.; Wong, J. Y.; Xing, X.; Xiang, N.; Wu, Y.; Li, C.; Chen, Q.; Li, D.; Liu, T.; Zhao, J.; Liu, M.; Tu, W.; Chen, C.; Jin, L.; Yang, R.; Wang, Q.; Zhou, S.; Wang, R.; Liu, H.; Luo, Y.;

Liu, Y.; Shao, G.; Li, H.; Tao, Z.; Yang, Y.; Deng, Z.; Liu, B.; Ma, Z.; Zhang, Y.; Shi, G.; Lam, T. T. Y.; Wu, J. T.; Gao, G. F.; Cowling, B. J.; Yang, B.; Leung, G. M.; Feng, Z. Early transmission dynamics in Wuhan, China, of novel coronavirus-infected pneumonia. *N. Engl. J. Med.* **2020**, *382*, 1199−1207.

(5) Cao, B.; Wang, Y.; Wen, D.; Liu, W.; Wang, J. L.; Fan, G.; Ruan, L.; Song, B.; Cai, Y.; Wei, M.; Li, X.; Xia, J.; Chen, N.; Xiang, J.; Yu, T.; Bai, T.; Xie, X.; Zhang, L.; Li, C.; Yuan, Y.; Chen, H.; Li, H. D.; Huang, H.; Tu, S.; Gong, F.; Liu, Y.; Wei, Y.; Dong, C.; Zhou, F.; Gu, X.; Xu, J.; Liu, Z.; Zhang, Y.; Li, H.; Shang, L.; Wang, K.; Li, K.; Zhou, X.; Dong, X.; Qu, Z.; Lu, S.; Hu, X.; Ruan, S.; Luo, S.; Wu, J.; Peng, L.; Cheng, F.; Pan, L.; Zou, J.; Jia, C.; Wang, J.; Liu, X.; Wang, S.; Wu, X.; Ge, Q.; He, J.; Zhan, H.; Qiu, F.; Guo, L.; Huang, C.; Jaki, T.; Hayden, F. G.; Horby, P. W.; Zhang, D.; Wang, C. A trial of lopinavir-ritonavir in adults hospitalized with severe Covid-19. *N. Engl. J. Med.* **2020**, *382*, 1787−1799.

(6) Borba, M. G. S.; Val, F. F. A.; Sampaio, V. S.; Alexandre, M. A. A.; Melo, G. C.; Brito, M.; Mourao, M. P. G.; Brito-Sousa, J. D.; Baia-da-Silva, D.; Guerra, M. V. F.; Hajjar, L. A.; Pinto, R. C.; Balieiro, A. A. S.; Pacheco, A. G. F.; Santos, J. D. O.; Naveca, F. G.; Xavier, M. S.; Siqueira, A. M.; Schwarzbold, A.; Croda, J.; Nogueira, M. L.; Romero, G. A. S.; Bassat, Q.; Fontes, C. J.; Albuquerque, B. C.; Daniel-Ribeiro, C.-T.; Monteiro, W. M.; Lacerda, M. V. G. Effect of high vs low doses of chloroquine diphosphate as adjunctive therapy for patients hospitalized with severe acute respiratory syndrome coronavirus 2 (SARS-CoV-2) infection: a randomized clinical trial. *JAMA Netw. Open* **2020**, *3*, e208857 DOI: 10.1001/jamanetworkopen.2020.8857.

(7) Sheahan, T. P.; Sims, A. C.; Zhou, S.; Graham, R. L.; Pruijssers, A. J.; Agostini, M. L.; Leist, S. R.; Schäfer, A.; Dinnon, K. H.; Stevens, L. J.; Chappell, J. D.; Lu, X.; Hughes, T. M.; George, A. S.; Hill, C. S.; Montgomery, S. A.; Brown, A. J.; Bluemling, G. R.; Natchus, M. G.; Saindane, M.; Kolykhalov, A. A.; Painter, G.; Harcourt, J.; Tamin, A.; Thornburg, N. J.; Swanstrom, R.; Denison, M. R.; Baric, R. S. An orally bioavailable broad-spectrum antiviral inhibits SARS-CoV-2 in human airway epithelial cell cultures and multiple coronaviruses in mice. *Sci. Transl. Med.* **2020**, *12*, eabb5883.

(8) Burrage, D. R.; Koushesh, S.; Sofat, N. Immunomodulatory drugs in the management of SARS-CoV-2. *Front. Immunol.* **2020**, *11*, 1844.

(9) Song, Y.; Zhang, M.; Yin, L.; Wang, K.; Zhou, Y.; Zhou, M.; Lu, Y. COVID-19 treatment: close to a cure? A rapid review of pharmacotherapies for the novel coronavirus (SARS-CoV-2). *Int. J. Antimicrob. Agents* **2020**, *56*, 106080.

(10) Wang, M.; Cao, R.; Zhang, L.; Yang, X.; Liu, J.; Xu, M.; Shi, Z.; Hu, Z.; Zhong, W.; Xiao, G. Remdesivir and chloroquine effectively inhibit the recently emerged novel coronavirus (2019-nCoV) in vitro. *Cell Res.* **2020**, *30*, 269−271.

(11) Goldman, J. D.; Lye, D. C. B.; Hui, D. S.; Marks, K. M.; Bruno, R.; Montejano, R.; Spinner, C. D.; Galli, M.; Ahn, M. Y.; Nahass, R. G.; Chen, Y. S.; SenGupta, D.; Hyland, R. H.; Osinusi, A. O.; Cao, H.; Blair, C.; Wei, X.; Gaggar, A.; Brainard, D. M.; Towner, W. J.; Muñoz, J.; Mullane, K. M.; Marty, F. M.; Tashima, K. T.; Diaz, G.; Subramanian, A. Remdesivir for 5 or 10 days in patients with severe Covid-19. *N. Engl. J. Med.* **2020**, *383*, 1827−1837.

(12) Siegel, D.; Hui, H. C.; Doerffler, E.; Clarke, M. O.; Chun, K.; Zhang, L.; Neville, S.; Carra, E.; Lew, W.; Ross, B.; Wang, Q.; Wolfe, L.; Jordan, R.; Soloveva, V.; Knox, J.; Perry, J.; Perron, M.; Stray, K. M.; Barauskas, O.; Feng, J. Y.; Xu, Y.; Lee, G.; Rheingold, A. L.; Ray, A. S.; Bannister, R.; Strickley, R.; Swaminathan, S.; Lee, W. A.; Bavari, S.; Cihlar, T.; Lo, M. K.; Warren, T. K.; Mackman, R. L. Discovery and synthesis of a phosphoramidate prodrug of a pyrrolo[2,1-f][triazin-4-amino] adenine C-nucleoside (GS-5734) for the treatment of Ebola and emerging viruses. *J. Med. Chem.* **2017**, *60*, 1648−1661.

(13) Brown, A. J.; Won, J. J.; Graham, R. L.; Dinnon, K. H., 3rd; Sims, A. C.; Feng, J. Y.; Cihlar, T.; Denison, M. R.; Baric, R. S.; Sheahan, T. P. Broad spectrum antiviral remdesivir inhibits human endemic and zoonotic deltacoronaviruses with a highly divergent RNA dependent RNA polymerase. *Antiviral Res.* **2019**, *169*, 104541.

(14) Wang, Q.; Wu, J.; Wang, H.; Gao, Y.; Liu, Q.; Mu, A.; Ji, W.; Yan, L.; Zhu, Y.; Zhu, C.; Fang, X.; Yang, X.; Huang, Y.; Gao, H.; Liu, F.; Ge, J.; Sun, Q.; Yang, X.; Xu, W.; Liu, Z.; Yang, H.; Lou, Z.; Jiang, B.; Guddat, L. W.; Gong, P.; Rao, Z. Structural basis for RNA replication by the SARS-CoV-2 polymerase. *Cell* **2020**, *182*, 417−428.

(15) Beigel, J. H.; Tomashek, K. M.; Dodd, L. E.; Mehta, A. K.; Zingman, B. S.; Kalil, A. C.; Hohmann, E.; Chu, H. Y.; Luetkemeyer, A.; Kline, S.; Lopez de Castilla, D.; Finberg, R. W.; Dierberg, K.; Tapson, V.; Hsieh, L.; Patterson, T. F.; Paredes, R.; Sweeney, D. A.; Short, W. R.; Touloumi, G.; Lye, D. C.; Ohmagari, N.; Oh, M. D.; Ruiz-Palacios, G. M.; Benfield, T.; Fätkenheuer, G.; Kortepeter, M. G.; Atmar, R. L.; Creech, C. B.; Lundgren, J.; Babiker, A. G.; Pett, S.; Neaton, J. D.; Burgess, T. H.; Bonnett, T.; Green, M.; Makowski, M.; Osinusi, A.; Nayak, S.; Lane, H. C. ACTT-1 Study Group Members. Remdesivir for the treatment of Covid-19 — final report. *N. Engl. J. Med.* **2020**, *383*, 1813−1826.

(16) The Food and Drug Administration. https://www.fda.gov/drugs/news-events-human-drugs/remdesivir-veklury-approval-treatment-covid-19-evidence-safety-and-efficacy (accessed 2020-12-20).

(17) Pan, H.; Peto, R.; Karim, Q. A.; Alejandria, M.; Henao-Restrepo, A. M.; García, C. H.; Kieny, M.-P.; Malekzadeh, R.; Murthy, S.; Preziosi, M.-P.; Reddy, S.; Periago, M. R.; Sathiyamoorthy, V.; Røttingen, J.-A.; Swaminathan, S. Repurposed antiviral drugs for COVID-19−interim WHO solidarity trial results. *MedRxiv* **2020**. DOI: 10.1101/2020.10.15.20209817

(18) Alanazi, A. S.; James, E.; Mehellou, Y. The ProTide prodrug technology: where next? *ACS Med. Chem. Lett.* **2019**, *10*, 2−5.

(19) McGuigan, C.; Cahard, D.; Sheeka, H. M.; De Clercq, E.; Balzarini, J. Aryl phosphoramidate derivatives of d4T have improved anti-HIV efficacy in tissue culture and may act by the generation of a novel intracellular metabolite. *J. Med. Chem.* **1996**, *39*, 1748−1753.

(20) Cho, A.; Saunders, O. L.; Butler, T.; Zhang, L.; Xu, J.; Vela, J. E.; Feng, J. Y.; Ray, A. S.; Kim, C. U. Synthesis and antiviral activity of a series of 1′-substituted 4-aza-7,9-dideazaadenosine C-nucleosides. *Bioorg. Med. Chem. Lett.* **2012**, *22*, 2705−2707.

(21) Murakami, E.; Wang, T.; Babusis, D.; Lepist, E. I.; Sauer, D.; Park, Y.; Vela, J. E.; Shih, R.; Birkus, G.; Stefanidis, D.; Kim, C. U.; Cho, A.; Ray, A. S. Metabolism and pharmacokinetics of the anti-hepatitis C virus nucleotide prodrug GS-6620. *Antimicrob. Agents Chemother.* **2014**, *58*, 1943−1951.

(22) Murakami, E.; Tolstykh, T.; Bao, H.; Niu, C.; Steuer, H. M.; Bao, D.; Chang, W.; Espiritu, C.; Bansal, S.; Lam, A. M.; Otto, M. J.; Sofia, M. J.; Furman, P. A. Mechanism of activation of PSI-7851 and its diastereoisomer PSI-7977. *J. Biol. Chem.* **2010**, *285*, 34337−34347.

(23) Davis, M. R.; Pham, C. U.; Cies, J. J. Remdesivir and GS-441524 plasma concentrations in patients with end-stage renal disease on haemodialysis. *J. Antimicrob. Chemother.* **2020**. DOI: 10.1093/jac/dkaa472.

(24) Tempestilli, M.; Caputi, P.; Avataneo, V.; Notari, S.; Forini, O.; Scorzolini, L.; Marchioni, L.; Ascoli Bartoli, T.; Castilletti, C.; Lalle, E.; Capobianchi, M. R.; Nicastri, E.; D'Avolio, A.; Ippolito, G.; Agrati, C.; et al. Pharmacokinetics of remdesivir and GS-441524 in two critically ill patients who recovered from COVID-19. *J. Antimicrob. Chemother.* **2020**, *75*, 2977−2980.

(25) Humeniuk, R.; Mathias, A.; Cao, H.; Osinusi, A.; Shen, G.; Chng, E.; Ling, J.; Vu, A.; German, P. Safety, tolerability, and pharmacokinetics of remdesivir, an antiviral for treatment of COVID-19, in healthy subjects. *Clin. Transl. Sci.* **2020**, *13*, 896−906.

(26) Williamson, B. N.; Feldmann, F.; Schwarz, B.; Meade-White, K.; Porter, D. P.; Schulz, J.; van Doremalen, N.; Leighton, I.; Yinda, C. K.; Pérez-Pérez, L.; Okumura, A.; Lovaglio, J.; Hanley, P. W.; Saturday, G.; Bosio, C. M.; Anzick, S.; Barbian, K.; Cihlar, T.; Martens, C.; Scott, D. P.; Munster, V. J.; de Wit, E. Clinical benefit of remdesivir in rhesus macaques infected with SARS-CoV-2. *Nature* **2020**, *585*, 273−276.

(27) Warren, T. K.; Jordan, R.; Lo, M. K.; Ray, A. S.; Mackman, R. L.; Soloveva, V.; Siegel, D.; Perron, M.; Bannister, R.; Hui, H. C.; Larson, N.; Strickley, R.; Wells, J.; Stuthman, K. S.; Van Tongeren, S.

A.; Garza, N. L.; Donnelly, G.; Shurtleff, A. C.; Retterer, C. J.; Gharaibeh, D.; Zamani, R.; Kenny, T.; Eaton, B. P.; Grimes, E.; Welch, L. S.; Gomba, L.; Wilhelmsen, C. L.; Nichols, D. K.; Nuss, J. E.; Nagle, E. R.; Kugelman, J. R.; Palacios, G.; Doerffler, E.; Neville, S.; Carra, E.; Clarke, M. O.; Zhang, L.; Lew, W.; Ross, B.; Wang, Q.; Chun, K.; Wolfe, L.; Babusis, D.; Park, Y.; Stray, K. M.; Trancheva, I.; Feng, J. Y.; Barauskas, O.; Xu, Y.; Wong, P.; Braun, M. R.; Flint, M.; McMullan, L. K.; Chen, S. S.; Fearns, R.; Swaminathan, S.; Mayers, D. L.; Spiropoulou, C. F.; Lee, W. A.; Nichol, S. T.; Cihlar, T.; Bavari, S. Therapeutic efficacy of the small molecule GS-5734 against Ebola virus in rhesus monkeys. *Nature* **2016**, *531*, 381−385.

(28) Lo, M. K.; Jordan, R.; Arvey, A.; Sudhamsu, J.; Shrivastava-Ranjan, P.; Hotard, A. L.; Flint, M.; McMullan, L. K.; Siegel, D.; Clarke, M. O.; Mackman, R. L.; Hui, H. C.; Perron, M.; Ray, A. S.; Cihlar, T.; Nichol, S. T.; Spiropoulou, C. F. GS-5734 and its parent nucleoside analog inhibit Filo-, Pneumo-, and Paramyxoviruses. *Sci. Rep.* **2017**, *7*, 43395.

(29) Mumtaz, N.; Jimmerson, L. C.; Bushman, L. R.; Kiser, J. J.; Aron, G.; Reusken, C.; Koopmans, M. P. G.; van Kampen, J. J. A. Cell-line dependent antiviral activity of sofosbuvir against Zika virus. *Antiviral Res.* **2017**, *146*, 161−163.

(30) Murakami, E.; Niu, C.; Bao, H.; Micolochick Steuer, H. M.; Whitaker, T.; Nachman, T.; Sofia, M. A.; Wang, P.; Otto, M. J.; Furman, P. A. The mechanism of action of beta-D-2′-deoxy-2′-fluoro-2′-C-methylcytidine involves a second metabolic pathway leading to beta-D-2′-deoxy-2′-fluoro-2′-C-methyluridine 5′-triphosphate, a potent inhibitor of the hepatitis C virus RNA-dependent RNA polymerase. *Antimicrob. Agents Chemother.* **2008**, *52*, 458−464.

(31) Agostini, M. L.; Andres, E. L.; Sims, A. C.; Graham, R. L.; Sheahan, T. P.; Lu, X.; Smith, E. C.; Case, J. B.; Feng, J. Y.; Jordan, R.; Ray, A. S.; Cihlar, T.; Siegel, D.; Mackman, R. L.; Clarke, M. O.; Baric, R. S.; Denison, M. R. Coronavirus susceptibility to the antiviral remdesivir (GS-5734) is mediated by the viral polymerase and the proofreading exoribonuclease. *mBio* **2018**, *9*, No. e00221-18.

(32) Murphy, B. G.; Perron, M.; Murakami, E.; Bauer, K.; Park, Y.; Eckstrand, C.; Liepnieks, M.; Pedersen, N. C. The nucleoside analog GS-441524 strongly inhibits feline infectious peritonitis (FIP) virus in tissue culture and experimental cat infection studies. *Vet. Microbiol.* **2018**, *219*, 226−233.

(33) Dickinson, P. J.; Bannasch, M.; Thomasy, S. M.; Murthy, V. D.; Vernau, K. M.; Liepnieks, M.; Montgomery, E.; Knickelbein, K. E.; Murphy, B.; Pedersen, N. C. Antiviral treatment using the adenosine nucleoside analogue GS-441524 in cats with clinically diagnosed neurological feline infectious peritonitis. *J. Vet. Intern. Med.* **2020**, *34*, 1587−1593.

(34) Pruijssers, A. J.; George, A. S.; Schäfer, A.; Leist, S. R.; Gralinksi, L. E.; Dinnon, K. H.; Yount, B. L.; Agostini, M. L.; Stevens, L. J.; Chappell, J. D.; Lu, X.; Hughes, T. M.; Gully, K.; Martinez, D. R.; Brown, A. J.; Graham, R. L.; Perry, J. K.; Du Pont, V.; Pitts, J.; Ma, B.; Babusis, D.; Murakami, E.; Feng, J. Y.; Bilello, J. P.; Porter, D. P.; Cihlar, T.; Baric, R. S.; Denison, M. R.; Sheahan, T. P. Remdesivir inhibits SARS-CoV-2 in human lung cells and chimeric SARS-CoV expressing the SARS-CoV-2 RNA polymerase in mice. *Cell Rep.* **2020**, *32*, 107940.

(35) Yan, V. C.; Muller, F. L. Advantages of the parent nucleoside GS-441524 over remdesivir for Covid-19 treatment. *ACS Med. Chem. Lett.* **2020**, *11*, 1361−1366.

(36) Avataneo, V.; de Nicolo, A.; Cusato, J.; Antonucci, M.; Manca, A.; Palermiti, A.; Waitt, C.; Walimbwa, S.; Lamorde, M.; di Perri, G.; D'Avolio, A. Development and validation of a UHPLC-MS/MS method for quantification of the prodrug remdesivir and its metabolite GS-441524: a tool for clinical pharmacokinetics of SARS-CoV-2/COVID-19 and Ebola virus disease. *J. Antimicrob. Chemother.* **2020**, *75*, 1772−1777.

(37) National Center for Advancing Translational Sciences. https://opendata.ncats.nih.gov/covid19/GS-441524. (accessed 2020-12-20).

(38) Israelow, B.; Song, E.; Mao, T.; Lu, P.; Meir, A.; Liu, F.; Alfajaro, M. M.; Wei, J.; Dong, H.; Homer, R. J.; Ring, A.; Wilen, C. B.; Iwasaki, A. Mouse model of SARS-CoV-2 reveals inflammatory role of type I interferon signaling. *J. Exp. Med.* **2020**, *217*, No. e20201241.

(39) Sun, J.; Zhuang, Z.; Zheng, J.; Li, K.; Wong, R. L.; Liu, D.; Huang, J.; He, J.; Zhu, A.; Zhao, J.; Li, X.; Xi, Y.; Chen, R.; Alshukairi, A. N.; Chen, Z.; Zhang, Z.; Chen, C.; Huang, X.; Li, F.; Lai, X.; Chen, D.; Wen, L.; Zhuo, J.; Zhang, Y.; Wang, Y.; Huang, S.; Dai, J.; Shi, Y.; Zheng, K.; Leidinger, M. R.; Chen, J.; Li, Y.; Zhong, N.; Meyerholz, D. K.; McCray, P. B., Jr.; Perlman, S.; Zhao, J. Generation of a broadly useful model for COVID-19 pathogenesis, vaccination, and treatment. *Cell* **2020**, *182*, 734−743.

(40) Körner, R. W.; Majjouti, M.; Alcazar, M. A. A.; Mahabir, E. Of mice and men: the coronavirus MHV and mouse models as a translational approach to understand SARS-CoV-2. *Viruses* **2020**, *12*, 880.

(41) Navas, S.; Seo, S. H.; Chua, M. M.; Das Sarma, J.; Lavi, E.; Hingley, S. T.; Weiss, S. R. Murine coronavirus spike protein determines the ability of the virus to replicate in the liver and cause hepatitis. *J. Virol.* **2001**, *75*, 2452−2457.

(42) McMahon, J. H.; Udy, A.; Peleg, A. Y. Remdesivir for the treatment of Covid-19 - preliminary report. *N. Engl. J. Med.* **2020**, *383*, 992−993.

(43) Yan, V. C.; Muller, F. L. Captisol and GS-704277, but not GS-441524, are credible mediators of remdesivir's nephrotoxicity. *Antimicrob. Agents Chemother.* **2020**, *64*, No. 01920.

(44) Pedersen, N. C.; Perron, M.; Bannasch, M.; Montgomery, E.; Murakami, E.; Liepnieks, M.; Liu, H. Efficacy and safety of the nucleoside analog GS-441524 for treatment of cats with naturally occurring feline infectious peritonitis. *J. Feline Med. Surg* **2019**, *21*, 271−281.

(45) Ng, B.; Cash-Mason, T.; Wang, Y.; Seitzer, J.; Burchard, J.; Brown, D.; Dudkin, V.; Davide, J.; Jadhav, V.; Sepp-Lorenzino, L.; Cejas, P. J. Intratracheal administration of siRNA triggers mRNA silencing in the lung to modulate T cell immune response and lung inflammation. *Mol. Ther.–Nucleic Acids* **2019**, *16*, 194−205.

https://dx.doi.org/10.1021/acs.jmedchem.0c01929
J. Med. Chem. XXXX, XXX, XXX−XXX